The Journal of Physical Chemistry Letters

Letter

Imaging van der Waals Interactions

Zhumin Han, Xinyuan Wei, Chen Xu, Chi-lun Chiang, Yanxing Zhang, Ruqian Wu, and Wilson Ho

J. Phys. Chem. Lett., **Just Accepted Manuscript** • DOI: 10.1021/acs.jpclett.6b02749 • Publication Date (Web): 02 Dec 2016

ACS Publications

The Journal of Physical Chemistry Letters is published by the American Chemical Society. 1155 Sixteenth Street N.W., Washington, DC 20036

Imaging van der Waals Interactions

Zhumin Han,[1] Xinyuan Wei,[1,2] Chen Xu,[1] Chi-lun Chiang,[1] Yanxing Zhang,[1,3] Ruqian Wu,[1] and W. Ho[1,4,]*

[1]*Department of Physics and Astronomy, University of California, Irvine, CA 92697-4575*

[2]*State Key Laboratory of Surface Physics and Key Laboratory for Computational Physical Sciences (MOE) & Department of Physics, Fudan University, Shanghai, China 200433*

[3]*College of Physics and Materials Science, Henan Normal University, Xinxiang, Henan, China 453007*

[4]*Department of Chemistry, University of California, Irvine, CA 92697-2025*

[*] To whom correspondence should be addressed. Electronic mail: wilsonho@uci.edu

ABSTRACT: The van der Waals interactions are responsible for a large diversity of structures and functions in chemistry, biology, and materials. Discussion of van der Waals interactions has focused on the attractive potential energy that varies as the inverse power of the distance between the two interacting partners. The origin of the attractive force is widely discussed as due to the correlated fluctuations of electron charges that lead to instantaneous dipole induced dipole attractions. Here, we use the inelastic tunneling probe to image the potential energy surface associated with the van der Waals interactions of xenon atoms.

TOC GRAPHICS

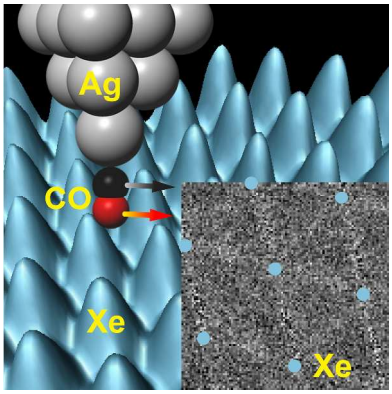

KEYWORDS: van der Waals interaction, chemical bond, inelastic tunneling probe, xenon self-assembly, scanning tunneling microscope, inelastic electron tunneling spectroscopy.

Chemical interactions underpin the formation of molecules from atoms and the self-assembly of extended atomic and molecular structures. The van der Waal's (vdW) bond is the weakest compared to the other types of bonds: covalent, ionic, metallic, and hydrogen. While individual vdW bond is weak, the interactions are additive and can become a significant binding force for an ensemble of atoms and molecules. Current description of the vdW bond does not implicate the sharing of electrons. The vdW potential energy arising from fluctuating charges and instantaneous dipoles exhibits inverse power law decays on the distance between the interacting partners. Despite the prevalence of vdW interactions, a proper experimental visualization combined with theoretical description remains elusive.[1]

For the inert gas atoms with spherically symmetric closed shells, vdW interactions are dominant in their bonding. In comparison, bonds involving carbon atoms are described by hybridized orbitals that have well-defined bonding directions, both in the number of bonds and angles between them. Consequently, molecules with carbon bonds are depicted schematically by skeletal structures that convey the locations of atoms and connections between them. The nature of such structures has only recently been experimentally shown by imaging the connections between atoms as lines in cyclic organic molecules by the atomic force microscope (AFM),[2–4] and cyclic organometallic molecules by the scanning tunneling microscope (STM).[5] Images of such lines indicate the presence of anisotropic potential associated with the charge distribution in the chemical bond. Self-assembly of Xe atoms on a metal surface presents an ideal vdW system for fundamental studies. The fact that they form a close packed hexagonal structure suggests the presence of interatomic attraction that is responsible for the self-assembly.

This paper provides new understanding into the nature of the vdW interactions through real space imaging of the potential energy surface (PES) and analyses by density functional calculations.

The inert gas atoms interact predominantly through vdW interactions. The large polarizability of Xe leads to favorable interaction strengths with its neighbors to form stable adsorption structures. Numerous studies have shown that Xe atoms form close packed self-assembled monolayer when dosed onto metal surfaces with different crystallographic orientations.[6,7] This behavior suggests that the self-assembled Xe structure is insensitive to the substrate symmetry and driven by interatomic interactions.

The adsorption of Xe monolayer on Ag(110) has been studied by low energy electron diffraction[8] and He atom scattering.[9] In the present experiment, islands of ordered Xe atoms are formed on the Ag(110) surface, as shown in Figure 1a where the Xe atoms can be seen to cover over a step. A zoom-in of the monolayer island in Figure 1b shows clearly the individual Xe atoms, their adsorption sites, and the larger unit cell for the Xe monolayer compared to the underlying unit cell of Ag(110). The Xe atoms are not in perfect registry with the Ag(110) lattice, indicating that the interaction within the Xe layer competes with the binding to the substrate. Contrary to previous DFT calculations with vdW interactions, the Xe atoms do not adsorb on top of a Ag atom,[10,11] but prefer the higher coordination sites.

When the bare tip is set closer to the surface (close set point), individual Xe atoms remain well resolved in Figure 1c and Figure 1d. Using the same set point defined by the bias voltage and current for Figure 1e as in Figure 1a and Figure 1b (far set point), no significant change is

observed with a CO-tip. However, the topographic image with the CO-tip in Figure 1f is qualitatively changed when the CO-tip is set closer to the surface as in Figure 1c. Specifically, each Xe atom is imaged as a dot and additionally a line appears and joins the centers of each pair of nearest neighbor atoms. These features cannot be due to effects of the substrate since the Xe overlayer has hexagonal symmetry while the underlying Ag(110) substrate has rectangular symmetry.

Another method to image the pattern of lines connecting the Xe atoms uses the itProbe,[5] as illustrated schematically in Figure 2a. In itProbe, a CO molecule is transferred from the surface to the tip and its presence at the end of the tip is confirmed by changes from the bare tip in the enhanced topographic images of adsorbed molecules and the characteristic CO vibrational spectrum by inelastic electron tunneling spectroscopy (IETS). The lowest energy vibrational mode of the CO-tip corresponds to the hindered or frustrated translational mode depicted in Figure 2a. The CO-tip can be positioned directly over a Xe atom or above the three-fold hollow site, as indicated in Figure 2b. The spectrum for the hindered translational mode of the CO shows spatial variations, as is exemplified by the spectra in Figure 2c for these two sites. This spatial dependence gives rise to itProbe images that derive from the spatial variations of the vibrational intensity of CO at a selected energy, as illustrated for 1.6 meV in Figure 2d. Similar to the topographic image shown in Figure 1f, a hexagonal pattern is revealed by the itProbe, with lines connecting the centers of nearest neighbor Xe atoms. Such a pattern extends over the entire island of self-assembled Xe atoms, as shown by the itProbe image in Figure 2f.

Disorder of the Xe atoms in the island can be induced by coadsorption with hexafluorobenzene (C_6F_6), as shown by the topographic image in Figure 3a and a close-up view in Figure 3b. When the CO-tip is set closer to the surface, lines connecting the nearest neighbor Xe atoms appear in the topographic image at constant current (Figure 3c) and in the current image at constant height (Figure 3d). The same pattern of lines is seen in the differential conductance *dI/dV* image (Figure 3e) and the itProbe d^2I/dV^2 image (Figure 3f). These images show lines connecting nearest neighbor Xe atoms, following their disordered positions. In contrast to covalent bonds involving carbon atoms, interactions among Xe atoms are not constrained by the angle subtended between adjacent lines.

Spectroscopy has shown the binding of a noble gas atom with a benzene molecule by vdW forces to form a stable complex in a molecular beam.[12] A noble gas atom can also bind to an acid via the acidic hydrogen.[13] Xenon compounds have been synthesized, including xenon fluorides[14] and complexes with a metal atom.[15] Xenon hydrides have also been documented[16] that reveal its chemical versatility. The nature of the vdW interactions is visualized in the present study by probing a single Xe atom bonded to a single cobalt-phthalocyanine (CoPc) molecule, as shown by the topographic image in Figure 4a. The adsorption site of the Xe-CoPc complex is determined by resolving the surface atoms of Ag(110) with the CO-tip set closer to the surface compared to the tunneling gap in Figure 4a. The differential conductance *dI/dV* image in Figure 4b suggests lines connecting the Xe atom to the CoPc molecule. The Xe-CoPc interactions are more clearly seen in the itProbe image in Figure 4c, as three lines connecting the center of the Xe atom to its three nearest neighbors: the H atoms in the two C-H bonds and

the N lone electron pair of the CoPc. A schematic diagram of the itProbe image is illustrated in Figure 4d. Similar to the disordered Xe atoms in the island of Figure 3, vdW interactions are not constrained by valence and angle as in covalent bonds formed by carbon.

Images of Xe atoms in self-assembly have been obtained on graphite[17] by the AFM and on Cu(110)[18] and Cu(111)[19] by the STM. In these and the present studies, growth of Xe islands initiates at step edges. Here using itProbe, the observed lines corresponding to the CoPc covalent structure and those connecting a Xe atom to its nearest neighbors in Xe islands and Xe-CoPc complex suggest a similarity in the description of covalent and vdW bonds.

Calculations for a free-standing Xe monolayer without substrate by DFT provide insights into the interactions within the Xe self-assembled layer and the origin of contrast in itProbe images. As shown in Figure 5a, the vdW interactions dominate the attractive forces within the Xe layer. The binding energy increases from 17 meV to 86 meV by including the vdW correction. The optimized distance between adjacent Xe atoms is 4.52 Å, in close agreement with the measured values of 4.60 Å to 4.67Å along different directions of the STM image in Figure 1b. The nature of the weak interactions between Xe atoms can be understood from the charge density difference shown in the inset of Figure 5a, $\rho_{Xe-lattice} - \rho_{Xe-atom}$. It is apparent that the electron density shifts from each nuclear region toward the region between two Xe atoms.

Chemical interactions between atoms are associated with the warp in space of the electrostatic potential. Consequently charges rearrange and bonding is correlated with an electronic shift to the region between two interacting atoms. Indeed, the nature of the vdW bond has been described in terms of the rearranged charge density,[20] such as the Ar dimer[21] and CH_4

dimer.[22] The lines observed for Xe interactions in the present work can be associated with the anisotropic charge arrangement in vdW bond as described by the vdW density functional theory.[1,21,22]

The various images of the topography (z), current (I), differential conductance (dI/dV), and itProbe (d^2I/dV^2) reflect the spatial variations of the interaction potential energy surface for the combined system of the CO-tip and the adsorbed species. The lines connecting Xe to CoPc in the itProbe image of Figure 4c have the same origin as the lines defining the skeletal structure of the covalent bonds in the CoPc molecule.[5] Additionally, the lines involving vdW interactions among Xe atoms are resolved in the z, I, and dI/dV images besides the d^2I/dV^2 itProbe images, as shown in Figure 1 to Figure 3 for the Xe islands.

In itProbe, the CO-tip is scanned over the adsorbed species and the d^2I/dV^2 signal is monitored at a chosen bias within the hindered translational mode of CO. The contrast in the itProbe d^2I/dV^2 images originates from variations in the peak position and intensity of the hindered translational mode of CO at different positions over the adsorbed species compared to over the Ag(110) substrate (background). These variations arise from the emergence of the coupling of the adsorbed species to the CO molecule attached to the tip. Instead of bonding only to the tip, the CO molecule is additionally influenced by the potential associated with the charge density of the species it probes.[5,23] In Figure 5b, a straight line prevails between two adjacent Xe atoms and corresponds to a ridge, or local maximum at least in one direction in the PES for the Ag-CO tip over the Xe layer. The CO bonded to the tip is under the influence of an

elastic restoring force $-k_1u$, with u representing a small lateral displacement for the hindered translational vibration. Interaction with the Xe layer adds a new restoring force on CO, $-k_2u$, and the vibrational energy changes to $\hbar\sqrt{(k_1+k_2)/m}$, where m is the effective mass of the motion. The negative curvature associated with ridges of PES implies that k_2 is negative and reduces the vibrational energy of CO by the diverging force on it over the Xe-Xe linkage. In contrast, a valley in the PES (positive curvature and k_2) is seen at each triangular hollow site of the Xe lattice, with a corresponding increase in the measured vibrational energy. Indeed, the spatial distribution of the PES curvature in Figure 5c, as related to k_2, maps well with the itProbe images in Figure 2d and 2f. By recording the inelastic electron tunneling signal at a reduced vibrational energy, the spatial map of the intensity for the CO hindered translational vibration yields contrast in the itProbe image that can be compared to the chemical structure and intermolecular interactions.

There have been recent debates on the origin of the intermolecular line features in nc-AFM images. A mechanical model has been introduced to account for the nc-AFM and itProbe images.[23,24] This model considers the tip-CO relaxation and describes the tip-sample interaction as the sum of pairwise Lennard-Jones potentials between the atoms constituting the molecule adsorbed on the substrate surface and the CO on the tip. However, further justification is required for the main conclusion of the model that intermolecular lines are merely the result of CO-tip relaxation without considering the enhanced electron density in the intermolecular region. For the total interaction energy, this model doesn't explicitly include contributions from the charge distribution of the molecule adsorbed on the substrate surface. However, the fact that

vdW coefficients (radius and energy) vary for the same elemental atom in different molecules or even at different sites in a molecule[25] indicates that these empirical parameters contain information on how that elemental atom is bonded differently with other atoms. Thus this model contains implicitly information on the charge distribution. In addition, results from the simulation sensitively rely on the various input parameters, such as atom positions, vdW coefficients, probe stiffness, and charge on the probe particle. The effects of CO relaxation could be easily overestimated if the empirical parameters are not fitted properly. This mechanical model cannot completely rule out the effect of the repulsive interaction caused by the enhanced charge density on either intermolecular bonds or intramolecular covalent bonds.

Hämäläinen *et al*. studied a self-assembled bis(para-pyridyl)acetylene (BPPA) molecular layer with nc-AFM and a sharp intermolecular line feature was observed between two nitrogen atoms of adjacent BPPA molecules.[26] This experiment is often cited to show that an intermolecular line feature in nc-AFM image does not represent a bond as suggested by the mechanical model. However, later studies have shown the existence of enhanced electron density distribution between the nitrogen atoms caused by the spatial overlap of electron lone pairs of the nitrogen atoms.[27,28] The short distance between these two nitrogen atoms on the Au(111) was induced by a surface mediated N-Au-N covalent bond that was not recognized previously.[28] Therefore this experiment cannot rule out the role of intermolecular electron density distribution on the sharp line features observed between nearby molecules.

In this paper, the itProbe images reflect the profile of the potential energy surface for a CO-tip interacting with assemblies of adsorbed species bonded together by vdW interactions.

The patterns resolved in the itProbe images reflect atoms in close proximity of each other in the formation of molecules through intramolecular interactions and in the self-assembly of atomic and molecular systems through much weaker vdW interactions. The tilting of the CO on the tip sharpens the contrast in these images and it should not be considered as the sole origin of the line features.

In summary, the positioning of a CO-tip over an adsorbed species sandwiches the CO molecule between the metal tip and the adsorbed species. Consequently, the CO molecule bonded to the metal tip experiences an additional interaction with the adsorbed species that can be tuned by adjusting the width of the tunneling gap. This additional interaction would cause a shift in the CO vibrational energy that is most clearly resolved for the lowest energy hindered translational mode. The magnitude of the shift exhibits an atomic-scale spatial dependence over different points of the adsorbed species. The vibrational energy of the CO relates to the curvature of the potential energy surface in the tunnel junction. The itProbe with a CO-terminated tip of a 600 mK STM measures the CO hindered translational vibration that senses the spatially varying potential of the adsorbed species. An image of the contour of constant curvature is obtained by mapping the vibrational intensity at a chosen vibrational energy. These itProbe images correlate with the skeletal structure of the adsorbed molecules and reveal perturbations of the PES in space that emerge from interactions among atoms and molecules.

In the present study, itProbe has been used to image the vdW interactions of Xe atoms in self-assembled islands and a Xe atom bonded to a Co-phthalocyanine molecule. Most notably,

lines of interactions are revealed, similar to those imaged for covalent bonds, except weaker in contrast.

Traditionally, vdW bond has been associated with charge fluctuations that lead to interactions of the instantaneous dipole with its induced counterpart in an adjacent entity. On the other hand, when atoms are in the vicinity of each other and the associated spatial anisotropy of the charge distribution, electron redistribution is bound to occur. Calculations by DFT with vdW correction reveal shift of electron density toward the region between adjacent Xe atoms. The itProbe images can be correlated with the ridges of the potential energy surface associated with the charge density. These results provide an understanding into the nature of chemical interactions as charge rearrangement between atoms and the associated perturbation of potential in space. Unlike covalent bond formed by carbon, the angle between two adjacent vdW interactions is not constrained and takes on values that depend on the positions of the adjacent atoms.

EXPERIMENTAL AND COMPUTATIONAL METHODS

All of the experiments were performed in ultrahigh vacuum ($< 5\times10^{-11}$ torr) with a home-built STM. The microscope was adapted in design from the one described in Ref. 29. Chemically etched sliver tips were used. The Ag(110) sample was repeatedly sputtered with Ne^+ and annealed at ~750 K. The tip was etched from polycrystalline silver wire and similarly sputtered and annealed in ultrahigh vacuum. For imaging the Xe-CoPc complex, cobalt phthalocyanine (CoPc) molecules were deposited onto the surface at ~25 K by thermal sublimation, followed by Xe and CO dosing. For forming disordered Xe islands,

hexafluorobenzene molecules were first dosed through a variable leak valve at ~25 K, followed by Xe and CO. Following dosing and prior to experiments, the STM scanner and the sample were further cooled to 600 mK with a single-shot ^{3}He sorption cryostat (Janis Research Co.). The transfer of CO from the surface to the tip follows a procedure similar to that described in Ref. 5, either with the tip stationary or scanning over the adsorbed CO. Detection of vibrational energy shifts for CO at different positions over the adsorbed species requires high energy resolution that is achieved by lowering the temperature to below 1 K for single-molecule IETS.[30] The image in Figure 2a is processed with WSxM software.[31]

We use two different operational modes of itProbe in this study: constant current mode and constant height mode. In constant current mode, feedback is turned off at the same tunneling set point for every pixel, followed by setting the sample bias to the imaging value, such as in Figure 2d. In constant height mode, feedback is turned off at a chosen location and sample bias is set to the imaging value prior to scanning. The feedback remains off during the whole imaging process. Tip can approach a chosen offset distance to the surface before imaging and retract by the same amount at the completion of imaging, such as in Figure 2f and Figure 3f. Alternatively, the tip can move toward the surface before data acquisition at each pixel and retract by the same distance prior to moving to the next pixel. This constant height mode minimizes the perturbation to the Xe-CoPc complex during the tip movement for Figure 4c. A detailed description of the different itProbe operational modes is given in Ref. 5.

First-principles DFT calculations were carried out by using the Vienna *ab initio* simulation package (VASP).[32] The exchange-correlation interactions among electrons were described at

the level of the generalized gradient approximation (GGA) with the Perdew, Burke, and Ernzerhof functional.[33] The optimized vdW correction term (optB86b-vdW) was invoked in all the calculations.[34] The energy cutoff for the plane wave basis expansion was set to 700 eV and the structures were fully relaxed until the forces on all atoms were smaller than 10^{-7} eV/Å. For the determination of the PES, we used a 2×2 supercell for the hexagonal Xe lattice and the CO-tip was modeled by a CO molecule attached to the vertex of a tetrahedron of four Ag atoms. The initial height of the O atom of CO before relaxation was set at 3.0 Å above the plane of the Xe layer. The Brillouin zone was sample by a 4×4×2k-mesh.

Two principal curvatures can be calculated at every point on a 2D surface.[35] We plot the smaller principal curvature of 2D PES in Figure 5c to highlight the apexes and ridges. The curvature mentioned in the main text without specification refers to the smaller principal curvature.

AUTHOR INFORMATION

Corresponding Author

*Email: wilsonho@uci.edu.

Notes

The authors declare no competing financial interests.

ACKNOWLEDGMENTS

The experimental work was supported by the Chemical Science, Geo- and Bioscience Division, Office of Science, U.S. Department of Energy, under Grant No. DE-FG02-04ER15595 (ZH, CJ) and DE-FG02-06ER15826 (CX). The theoretical work was supported by the Condensed Matter Physics Program, Division of Materials Research, National Science Foundation, under Grant No. DMR-1411338 (XW, YZ). Additionally, XW received support from the China Scholarship Council and the National Natural Science Foundation of China (Grant No. 61171011).

REFERENCES

(1) Berland, K.; Cooper, V. R.; Lee, K.; Schröder, E.; Thonhauser, T.; Hyldgaard, P.; Lundqvist, B. I. Van Der Waals Forces in Density Functional Theory: A Review of the vdW-DF Method. *Reports Prog. Phys.* **2015**, *78*, 66501.

(2) Gross, L.; Mohn, F.; Moll, N.; Liljeroth, P.; Meyer, G. The Chemical Structure of a Molecule Resolved by Atomic Force Microscopy. *Science* **2009**, *325*, 1110–1114.

(3) de Oteyza, D. G.; Gorman, P.; Chen, Y.-C.; Wickenburg, S.; Riss, A.; Mowbray, D. J.; Etkin, G.; Pedramrazi, Z.; Tsai, H.-Z.; Rubio, A.; Crommie, M. F.; Fischer, F. R. Direct Imaging of Covalent Bond Structure in Single-Molecule Chemical Reactions. *Science* **2013**, *340*, 1434–1437.

(4) Zhang, J.; Chen, P.; Yuan, B.; Ji, W.; Cheng, Z.; Qiu, X. Real-Space Identification of Intermolecular Bonding with Atomic Force Microscopy. *Science* **2013**, *342*, 611–614.

(5) Chiang, C.L.; Xu, C.; Han, Z.; Ho, W. Real-Space Imaging of Molecular Structure and Chemical Bonding by Single-Molecule Inelastic Tunneling Probe. *Science* **2014**, *344*, 885–888.

(6) Diehl, R. D.; Seyller, T.; Caragiu, M.; Leatherman, G. S.; Ferralis, N.; Pussi, K.; Kaukasoina, P.; Lindroos, M. The Adsorption Sites of Rare Gases on Metallic Surfaces: A Review. *J. Phys. Condens. Matter* **2004**, *16*, S2839–S2862.

(7) Bruch, L. W.; Diehl, R. D.; Venables, J. A. Progress in the Measurement and Modeling of Physisorbed Layers. *Rev. Mod. Phys.* **2007**, *79*, 1381–1454.

(8) Chesters, M. A.; Hussain, M.; Pritchard, J. Xenon Monolayer Structures on Copper and

Silver. *Surf. Sci.* **1973**, *35*, 161–171.

(9) Mason, B. .; Williams, B. . The Scattering of He from Adsorbed Layers of Gases on Ag(110). *Surf. Sci.* **1984**, *139*, 173–184.

(10) Silva, J. L. F. Da; Stampfl, C.; Scheffler, M. Adsorption of Xe Atoms on Metal Surfaces: New Insights from First-Principles Calculations. *Phys. Rev. Lett.* **2003**, *90*, 66104.

(11) Chen, D.-L.; Al-Saidi, W. A.; Johnson, J. K. The Role of van Der Waals Interactions in the Adsorption of Noble Gases on Metal Surfaces. *J. Phys. Condens. Matter* **2012**, *24*, 424211.

(12) Weber, T.; Riedle, E.; Neusser, H. J.; Schlag, E. W. Van Der Waals Bond Lengths and Electronic Spectral Shifts of the Benzene-Kr and Benzene-Xe Complexes. *Chem. Phys. Lett.* **1991**, *183*, 77–83.

(13) Gąszowski, D.; Ilczyszyn, M. Hydrogen Bonding to Xenon: A Comparison with Neon, Argon and Krypton Complexes. *Chem. Phys. Lett.* **2013**, *556*, 59–64.

(14) Li, W.-K.; Zhou, G.-D.; Wai Mak, T. C. Structural Chemistry of Group 17 and Group 18 Elements. In *Advanced Structural Inorganic Chemistry*; IUCr texts on crystallography; Oxford University Press: New York, 2008; pp 654–681.

(15) Seidel, S. Xenon as a Complex Ligand: The Tetra Xenono Gold(II) Cation in $AuXe_4^{2+}(Sb_2F_{11}^-)_2$. *Science* **2000**, *290*, 117–118.

(16) Khriachtchev, L.; Räsänen, M.; Gerber, R. B. Noble-Gas Hydrides: New Chemistry at Low Temperatures. *Acc. Chem. Res.* **2009**, *42*, 183–191.

(17) Allers, W.; Schwarz, A.; Schwarz, U. D.; Wiesendanger, R. Dynamic Scanning Force

Microscopy at Low Temperatures on a Noble-Gas Crystal: Atomic Resolution on the xenon(111) Surface. *Europhys. Lett.* **1999**, *48*, 276–279.

(18) Dienwiebel, M.; Zeppenfeld, P.; Einfeld, J.; Comsa, G.; Picaud, F.; Ramseyer, C.; Girardet, C. Effect of the Diffusion Anisotropy on the Nucleation and Growth of Xenon on Cu(110). *Surf. Sci.* **2000**, *446*, L113–L119.

(19) Park, J.-Y.; Ham, U. D.; Kahng, S.-J.; Kuk, Y.; Miyake, K.; Hata, K.; Shigekawa, H. Modification of Surface-State Dispersion upon Xe Adsorption: A Scanning Tunneling Microscope Study. *Phys. Rev. B* **2000**, *62*, R16341–R16344.

(20) Feynman, R. P. Forces in Molecules. *Phys. Rev.* **1939**, *56*, 340–343.

(21) Thonhauser, T.; Cooper, V. R.; Li, S.; Puzder, A.; Hyldgaard, P.; Langreth, D. C. Van Der Waals Density Functional: Self-Consistent Potential and the Nature of the van Der Waals Bond. *Phys. Rev. B* **2007**, *76*, 125112.

(22) Ferri, N.; DiStasio, R. A.; Ambrosetti, A.; Car, R.; Tkatchenko, A. Electronic Properties of Molecules and Surfaces with a Self-Consistent Interatomic van Der Waals Density Functional. *Phys. Rev. Lett.* **2015**, *114*, 176802.

(23) Hapala, P.; Temirov, R.; Tautz, F. S.; Jelínek, P. Origin of High-Resolution IETS-STM Images of Organic Molecules with Functionalized Tips. *Phys. Rev. Lett.* **2014**, *113*, 226101.

(24) Hapala, P.; Kichin, G.; Wagner, C.; Tautz, F. S.; Temirov, R.; Jelínek, P. Mechanism of High-Resolution STM/AFM Imaging with Functionalized Tips. *Phys. Rev. B* **2014**, *90*, 85421.

(25) Jorgensen, W. L.; Maxwell, D. S.; Tirado-Rives, J. Development and Testing of the OLPS All-Atom Force Field on Conformational Energetics and Properties of Organic Liquids. *J. Am. Chem. Soc.* **1996**, *118*, 11225–11236.

(26) Hämäläinen, S. K.; van der Heijden, N.; van der Lit, J.; Hartog, S. den; Liljeroth, P.; Swart, I.; den Hartog, S. Intermolecular Contrast in Atomic Force Microscopy Images without Intermolecular Bonds. *Phys. Rev. Lett.* **2014**, *113*, 186102.

(27) Guo, C.-S.; Xin, X.; Van Hove, M. A.; Ren, X.; Zhao, Y. Origin of the Contrast Interpreted as Intermolecular and Intramolecular Bonds in Atomic Force Microscopy Images. *J. Phys. Chem. C* **2015**, *119*, 14195–14200.

(28) Wang, C.-G.; Cheng, Z.-H.; Qiu, X.-H.; Ji, W. Unusually High Electron Density in an Intermolecular Non-Bonding Region: Role of Metal Substrate. *Chinese Chem. Lett.* **2016**. DOI: 10.1016/j.cclet.2016.08.004.

(29) Stipe, B. C.; Rezaei, M. A.; Ho, W. A Variable-Temperature Scanning Tunneling Microscope Capable of Single-Molecule Vibrational Spectroscopy. *Rev. Sci. Instrum.* **1999**, *70*, 137–143.

(30) Stipe, B. C.; Rezaei, M. A.; Ho, W. Single-Molecule Vibrational Spectroscopy and Microscopy. *Science* **1998**, *280*, 1732–1735.

(31) Horcas, I.; Fernández, R.; Gómez-Rodríguez, J. M.; Colchero, J.; Gómez-Herrero, J.; Baro, A. M. WSXM: A Software for Scanning Probe Microscopy and a Tool for Nanotechnology. *Rev. Sci. Instrum.* **2007**, *78*, 13705.

(32) Kresse, G.; Furthmüller, J. Efficiency of Ab-Initio Total Energy Calculations for Metals

and Semiconductors Using a Plane-Wave Basis Set. *Comput. Mater. Sci.* **1996**, *6*, 15–50.

(33) Perdew, J. P.; Burke, K.; Ernzerhof, M. Generalized Gradient Approximation Made Simple. *Phys. Rev. Lett.* **1996**, *77*, 3865–3868.

(34) Klimeš, J.; Bowler, D. R.; Michaelides, A. Chemical Accuracy for the van Der Waals Density Functional. *J. Phys. Condens. Matter* **2010**, *22*, 22201.

(35) Guggenheimer, H. W. Surfaces. In *Differential Geometry*; Dover Publications: New York, 1977; pp 206–260.

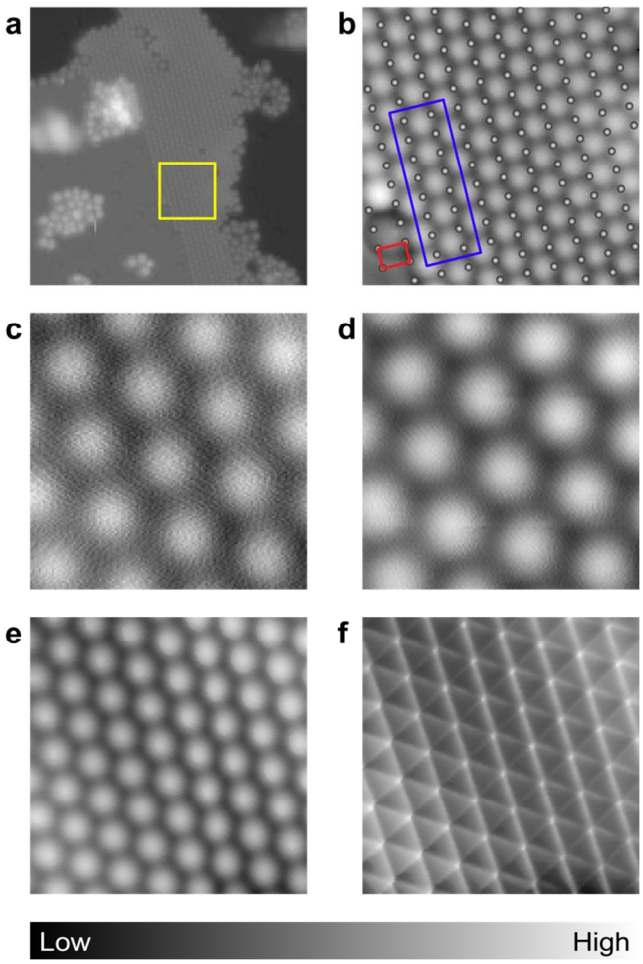

Figure 1. Constant current topographic images of self-assembled Xe island next to a step edge on Ag(110). **(**a) Bare-tip. Tunneling gap set with tunneling current 0.1 nA and sample bias 0.1 V. Brighter dots correspond mostly to C_6F_6 in the second layer. (b) Bare-tip. Zoom-in with the same set point of the area shown by the square in a. The large rectangle (blue) denotes the unit cell of the Xe monolayer; the unit cell of the Ag(110) substrate is indicated by the small rectangle (red). A step separates the two rectangles. The Ag atoms in the underlying substrate are indicated by the smaller open circles, as determined by resolving the Ag(110) lattice next to the Xe island with the CO-tip and extrapolating the Ag lattice positions to the Xe island. (c) Bare-tip. Tunneling gap decreased with set point 0.1 nA and 10 mV. (d) Bare-tip. Tunneling gap further decreased with set point 4 nA and 10 mV. (e) CO-tip. Set point 0.1 nA and 0.1 V (same as a and b). (f) CO-tip. Set point 0.1 nA and 10 mV (same as c). Most strikingly, the CO-tip reveals lines connecting the centers of adjacent Xe atoms; each Xe atom is connected to 6 Xe atoms in a close packed hexagonal symmetry.

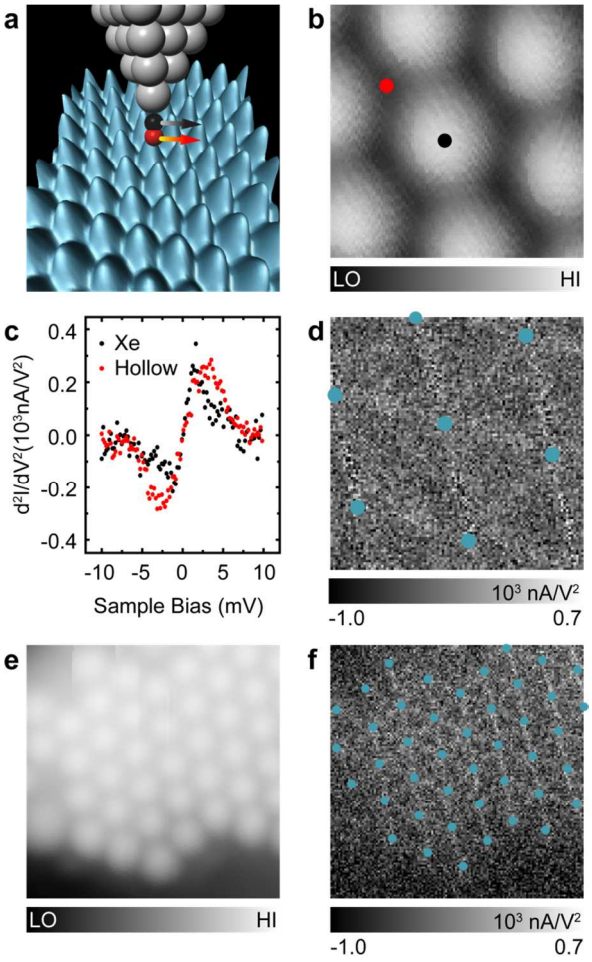

Figure 2. Imaging connectivity of vdW interactions with itProbe. (a) Schematic of itProbe showing the CO-tip over a self-assembled Xe monolayer (topographic image) while monitoring the hindered translational vibration of CO (C: black ball, O: red ball). (b) A topographic image obtained by a CO-tip with the tunneling gap set at 0.1 nA and 0.1 V, showing the hexagonal close pack arrangement of Xe atoms. (c) STM-IETS of CO-tip at set point 0.1 nA and 10 mV, showing the hindered translational mode, recorded at the two positions indicated in b: directly over a Xe atom (black dot) and over the triangular hollow site (red dot). (d**)** Constant current itProbe image of Xe atoms in b with bias set at 1.6 mV. At each pixel, the tunneling gap is chosen with set point 0.1 nA and 10 mV. Feedback is then turned off, followed by decreasing the bias to 1.6 mV for recording the d^2I/dV^2 vibrational signal. (e) Topographic image for part of a self-assembled island with set point 0.1 nA and 0.1 V. (f) Corresponding constant height itProbe image of the same area as e. The constant tunneling height is chosen with set point of 0.1 nA and 0.1 V over the central Xe atom, followed by turning off the feedback. Signal acquisition is initiated after decreasing the bias to 1.5 mV and bringing the tip 1.6 Å closer to the surface. For ease of visualization, the positions of the Xe atoms are indicted by the blue dots.

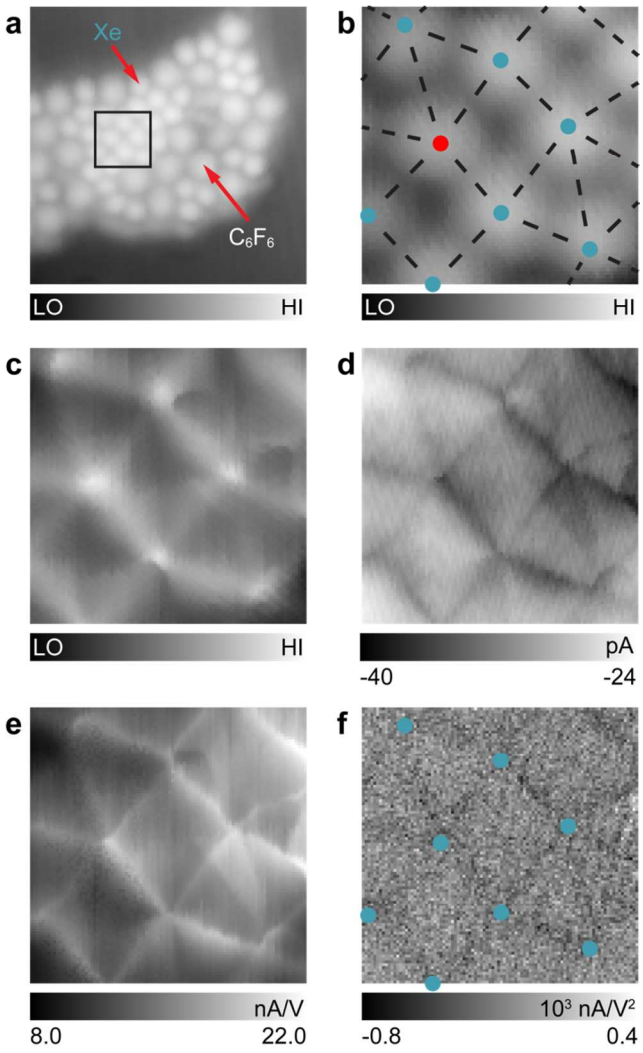

Figure 3. Imaging connectivity in disordered monolayer of Xe atoms with a CO-tip. (a) Topographic image of an island of Xe atoms with disorder caused by the coadsorption of hexafluorobenzene (C_6F_6), recorded with set point 0.1 nA and 0.1 V. (b) A zoom-in image of the area indicated by the square in a. Dots indicate the positions of the Xe atoms and dashed lines connect the centers of Xe atoms, showing different coordination numbers and angles subtended between adjacent Xe-Xe lines of interaction. (c) Topographic image with set point 0.1 nA and 10 mV for the same area as in b, revealing lines connecting Xe atoms. (d)-(f) Simultaneously acquired constant height imaging at -1.0 mV with set point 0.1 nA and 0.1 V over the center of the Xe atom indicated by the red dot in b, followed by turning the feedback off and advancing the tip 1.6 Å closer to the surface prior to imaging: (d) constant height current image, (e) differential conductance dI/dV image, and (f) itProbe d^2I/dV^2 image with blue dots indicating the positions of the Xe atoms. Figure 2d and Figure 3f have opposite contrast because they are imaged at opposite polarity of +1.6 mV and -1.0 mV, respectively.

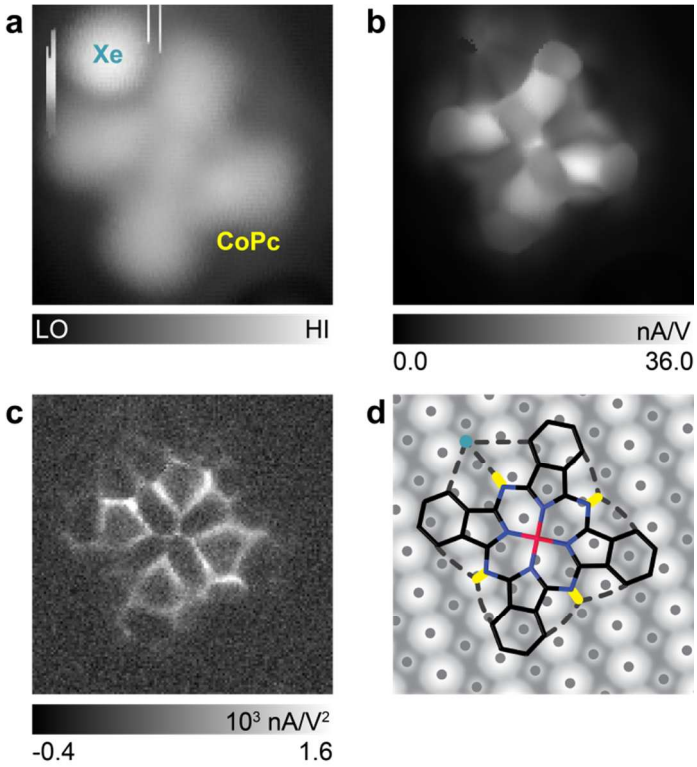

Figure 4. Interaction of a Xe atom with a cobalt phthalocyanine molecule. (a) Topographic image recorded with a CO-tip at set point 0.1 nA and 0.1 V. (b**)** Constant height *dI/dV* image with set point 0.3 nA and 0.1 V over the cobalt atom in CoPc, followed by turning the feedback off, lowering the bias to 1.5 mV, bringing the tip 1.3 Å closer to the surface prior to recording the image at each pixel, and retracting by the same distance before moving to the next pixel. (c**)** Simultaneously acquired itProbe image of the d^2I/dV^2 signal. (d**)** Schematic diagram of the interaction of Xe atom to its three nearest neighbors in CoPc: the lone pair (yellow segment) and the two H atoms in two nearest C-H bonds. The three dashed lines emanating from the center of Xe atom correspond to the lines seen in the itProbe image of c. Away from the region of the Xe atom, the other dashed lines indicate the interactions of H atoms in the two C-H bonds with each nitrogen lone pair of electrons.

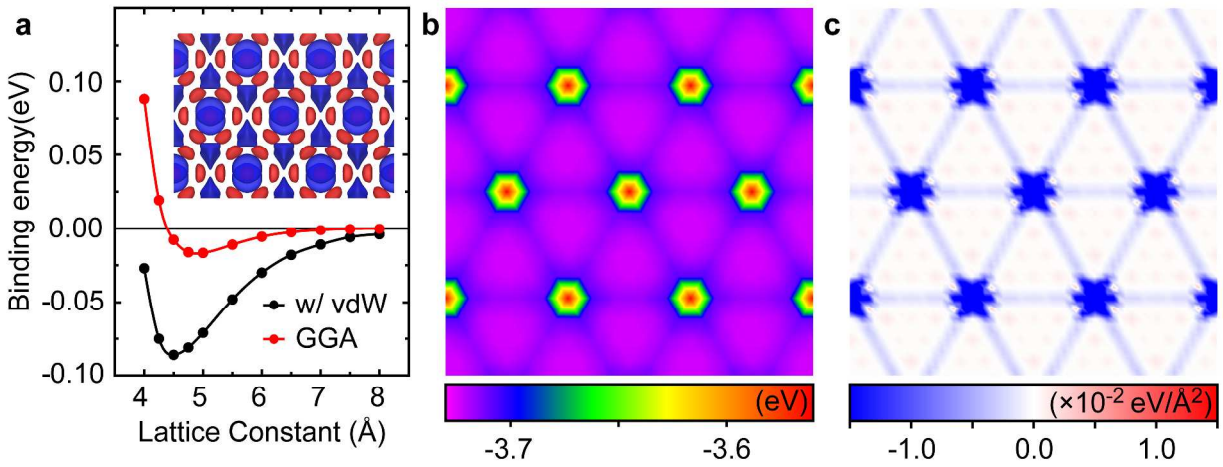

Figure 5. DFT analyses of Xe self-assembled monolayer. (a) Binding energy per unit cell of Xe atoms versus the hexagonal lattice constant: with (bottom black curve) and without (red curve) vdW correction. Inset shows the three dimensional isosurfaces of the charge density difference between Xe lattice and isolated Xe atoms, defined as $\rho_{Xe-lattice} - \rho_{Xe-atom}$, where red and blue colors indicate electron accumulation ($+2.5\times10^{-4}$ e/Å^3) and depletion (-2.5×10^{-4} e/Å^3), respectively. (b) The potential energy surface (PES) for Ag-CO tip and underlying Xe lattice, showing a ridge between adjacent pair of Xe atoms. (c) The smaller principal curvature of the 2D surface of PES in (b), showing lines of negative curvature between adjacent Xe atoms.

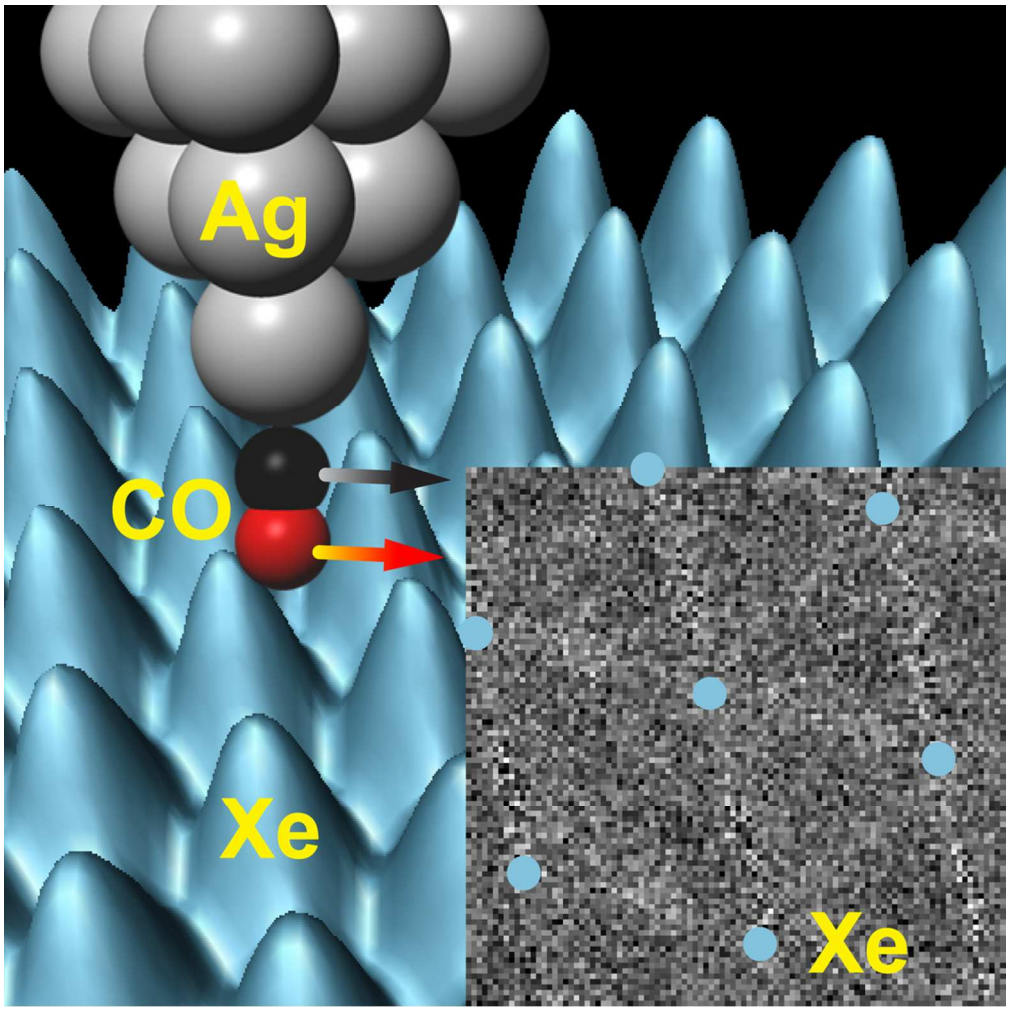

50x50mm (600 x 600 DPI)

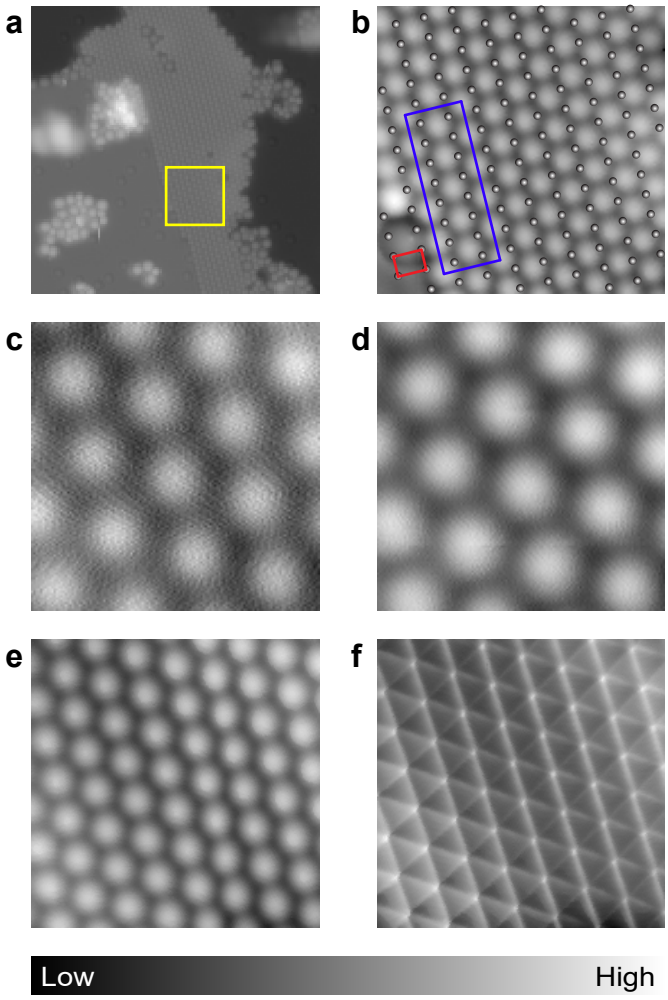
a
b
c
d
e
f
Low
High

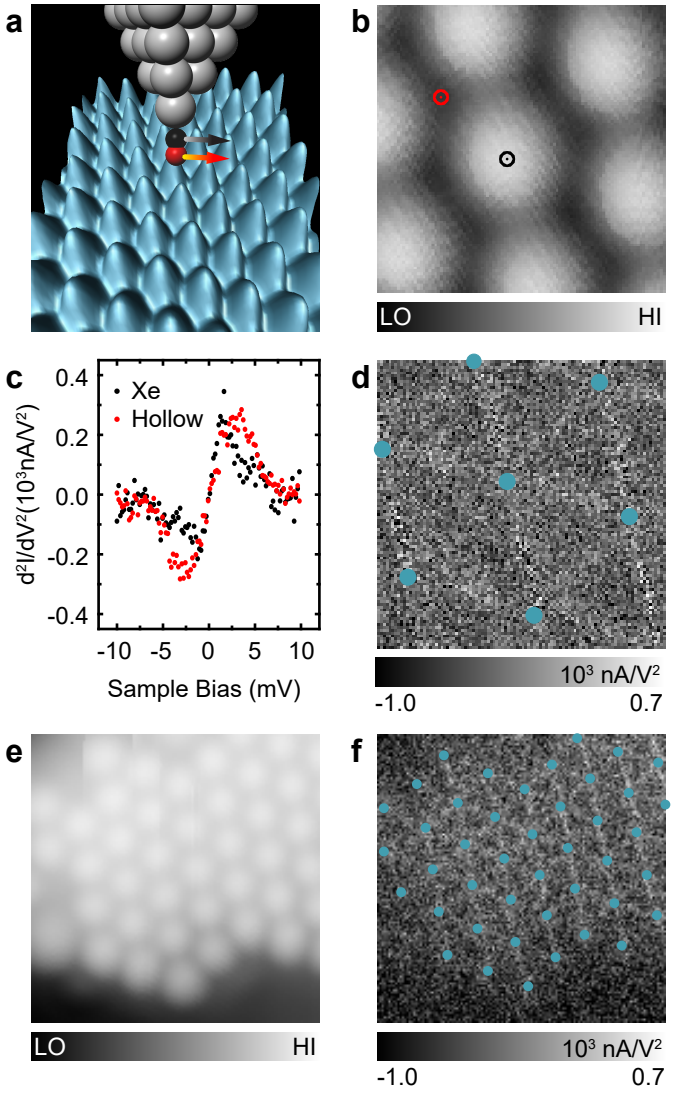
a
b
LO
HI
c
0.4
0.2
0.0
-0.2
-0.4
Xe
Hollow
d²I/dV²(10³nA/V²)
-10 -5 0 5 10
Sample Bias (mV)
d
10³ nA/V²
-1.0
0.7
e
LO
HI
f
10³ nA/V²
-1.0
0.7

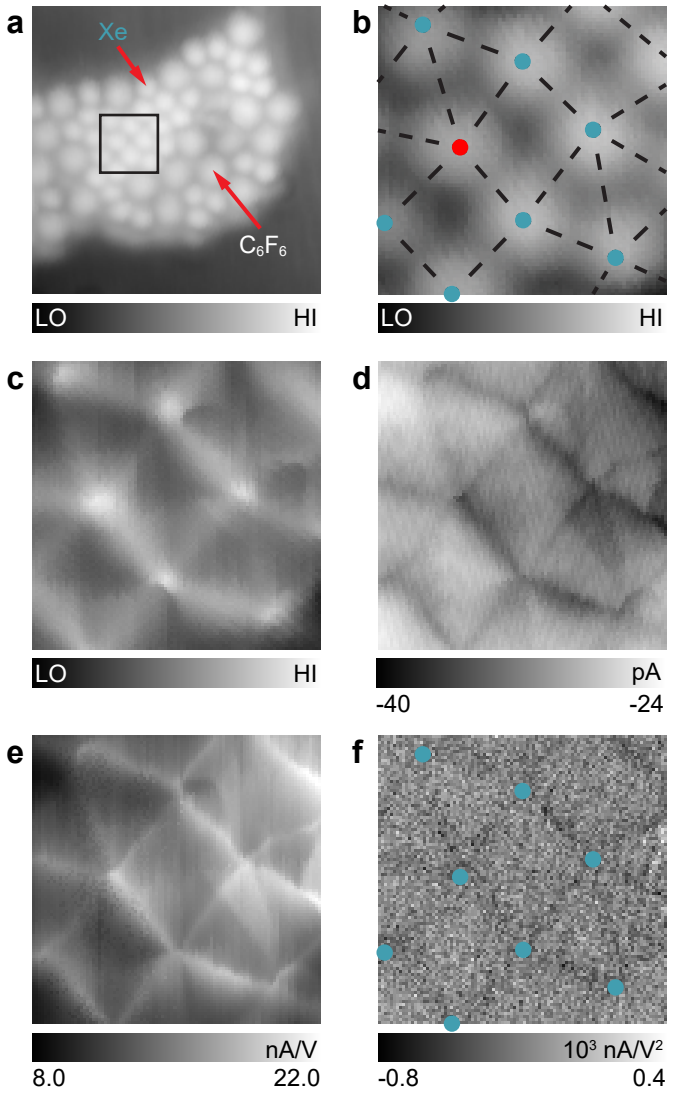
a
Xe
C_6F_6
LO
HI
b
LO
HI
c
LO
HI
d
pA
-40
-24
e
nA/V
8.0
22.0
f
10^3 nA/V^2
-0.8
0.4

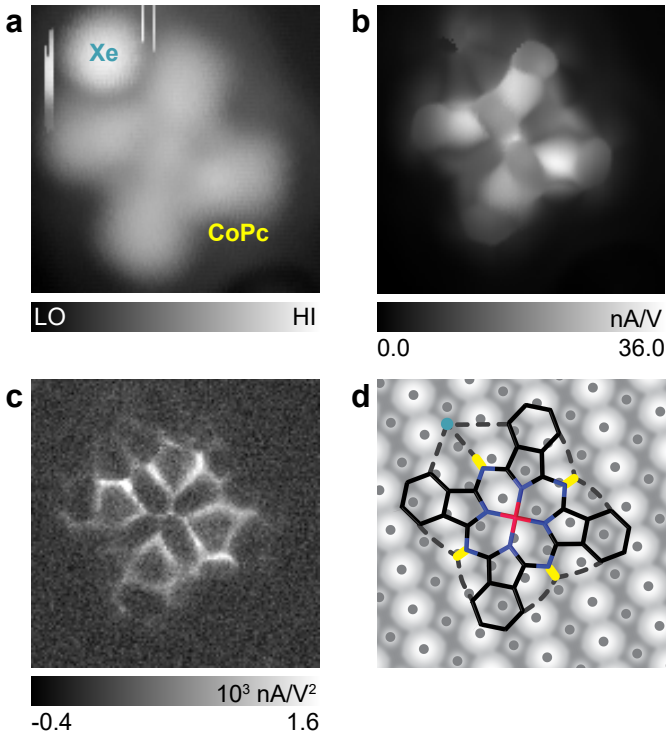
a
Xe
CoPc
LO
HI
b
nA/V
0.0
36.0
c
10³ nA/V²
-0.4
1.6
d

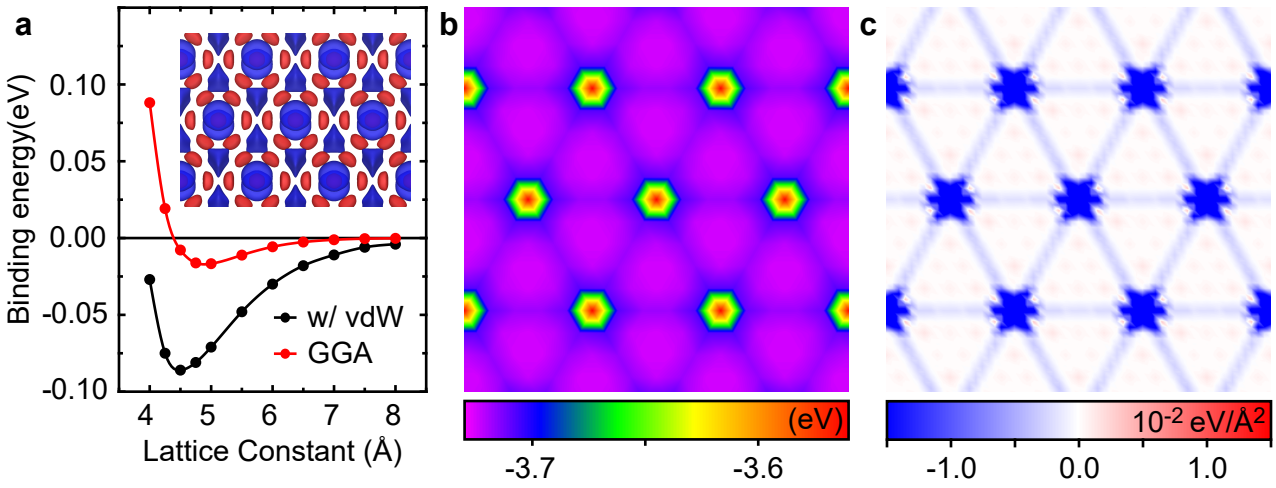
a
b
c
Binding energy(eV)
0.10
0.05
0.00
-0.05
-0.10
4
5
6
7
8
Lattice Constant (Å)
w/ vdW
GGA
(eV)
-3.7
-3.6
10-2 eV/Å2
-1.0
0.0
1.0